Defects, strain relaxation, and compositional grading in high indium content InGaN epilayers grown by molecular beam epitaxy

C. Bazioti, E. Papadomanolaki, Th. Kehagias, T. Walther, J. Smalc-Koziorowska, E. Pavlidou, Ph. Komninou, Th. Karakostas, E. Iliopoulos, and G. P. Dimitrakopulos

Citation: Journal of Applied Physics **118**, 155301 (2015); doi: 10.1063/1.4933276
View online: http://dx.doi.org/10.1063/1.4933276
View Table of Contents: http://scitation.aip.org/content/aip/journal/jap/118/15?ver=pdfcov
Published by the AIP Publishing

Defects, strain relaxation, and compositional grading in high indium content InGaN epilayers grown by molecular beam epitaxy

C. Bazioti,[1] E. Papadomanolaki,[2] Th. Kehagias,[1] T. Walther,[3] J. Smalc-Koziorowska,[4] E. Pavlidou,[1] Ph. Komninou,[1] Th. Karakostas,[1] E. Iliopoulos,[2] and G. P. Dimitrakopulos[1,a)]
[1]*Physics Department, Aristotle University of Thessaloniki, GR 541 24 Thessaloniki, Greece*
[2]*Microelectronics Research Group (MRG), IESL, FORTH, P.O. Box 1385, 71110 Heraklion Crete, Greece and Physics Department, University of Crete, Heraklion Crete, Greece*
[3]*Department of Electronic & Electrical Engineering, University of Sheffield, Sheffield S1 3JD, United Kingdom*
[4]*Institute of High Pressure Physics, Polish Academy of Sciences, Sokolowska 29/37, 01-142 Warsaw, Poland*

(Received 7 July 2015; accepted 3 October 2015; published online 16 October 2015)

We investigate the structural properties of a series of high alloy content InGaN epilayers grown by plasma-assisted molecular beam epitaxy, employing the deposition temperature as variable under invariant element fluxes. Using transmission electron microscopy methods, distinct strain relaxation modes were observed, depending on the indium content attained through temperature adjustment. At lower indium contents, strain relaxation by V-pit formation dominated, with concurrent formation of an indium-rich interfacial zone. With increasing indium content, this mechanism was gradually substituted by the introduction of a self-formed strained interfacial InGaN layer of lower indium content, as well as multiple intrinsic basal stacking faults and threading dislocations in the rest of the film. We show that this interfacial layer is not chemically abrupt and that major plastic strain relaxation through defect introduction commences upon reaching a critical indium concentration as a result of compositional pulling. Upon further increase of the indium content, this relaxation mode was again gradually succeeded by the increase in the density of misfit dislocations at the InGaN/GaN interface, leading eventually to the suppression of the strained InGaN layer and basal stacking faults. © *2015 AIP Publishing LLC*. [http://dx.doi.org/10.1063/1.4933276]

I. INTRODUCTION

$In_xGa_{1-x}N$ epitaxial films with high indium content are important for optoelectronics applications up to the near-infrared, as well as for high efficiency photovoltaics. The tailoring of the indium composition, in principle, permits bandgap tunability from 0.7 up to 3.4 eV, thus allowing utilization of most part of the solar spectrum.[1,2] However, due to the immiscibility of alloy constituents, chemically induced phenomena, such as phase separation and compositional pulling, may take place, resulting in complex defect microstructures that are sensitive to the growth conditions.[3–6]

The fluctuations in the indium concentration can be either long- or short-range in character. Short-range ones cause the local depletion of indium around regions that exhibit higher InN molar fraction. Elastic strain shifts the center of the miscibility gap to higher indium contents leading to the appearance of periodic compositional fluctuations.[7,8] Line and extended defects, such as threading dislocations (TDs), can induce local indium clustering.[9–13] On the other hand, compositional pulling is a mesoscale phenomenon, whereby the compressive strain due to the interfacial misfit impedes incorporation of the larger indium atoms, causing a gradually increasing indium concentration with increasing film thickness.[14]

Plasma-assisted molecular beam epitaxy (PAMBE), in principle, is a suitable growth method for achieving high ($x > 0.2$) indium contents. It can be employed in order to take advantage of metastability, and to avoid phase separation, by exploiting low growth temperatures (T_{gr}) so that the mobility of indium atoms is reduced.[15] Due to the easier dissociation of In-N bonds, indium incorporation is favored at $T_{gr} < 500\,^{\circ}C$.[15,16] On the other hand, the surfactant effect of the indium adlayer formed under metal enrichment of the surface favors the desired two-dimensional (2D) growth.[17] Iliopoulos *et al.*[18] have demonstrated PAMBE-growth of (0001) InGaN films over the entire composition range with high indium incorporation efficiency, using a low temperature range and almost stoichiometric flux ratios. Phase separation and a decrease of the indium content along the growth direction have been observed in PAMBE growth at higher temperatures.[19,20] Film growth at the indium accumulation limit and at temperatures where InGaN decomposition is active has been reported.[21]

The defect microstructure of the epilayer, in conjunction with the indium distribution and strain content, is crucial for device efficiency. The microstructure depends in a sensitive manner on the operating mechanisms for misfit relief, which, in turn, are affected by the growth kinetics. The concept of "critical thickness," h_{cr}, describes the response of the system to the stored elastic energy. The interplay between chemistry and available strain relaxation modes has been pointed out in multiple previous works that concern principally epilayers grown by metalorganic vapor phase epitaxy (MOVPE). Spinodal decomposition was reported in InGaN films with indium content $x \gtrsim 0.3$.[8] V-pit formation from TDs was

a)Author to whom correspondence should be addressed. Electronic mail: gdim@auth.gr.

reported as a mechanism of strain relaxation in films with $x \lesssim 0.15$, whereas pyramidal slip through the Matthews-Blakeslee mechanism[22] operated when the TD density was significantly reduced.[23,24] When free surfaces intercepted the epitaxial interface, e.g., due to pits, relaxation proceeded through basal slip of misfit dislocation half-loops.[25]

Below h_{cr} (according to the People-Bean model),[26] the film retains a principally elastic strain state and the compositional pulling phenomenon appears.[27,28] Above h_{cr}, reciprocal space x-ray diffraction (XRD) maps of asymmetrical reflections often exhibit double points associated with discontinuous strain relaxation along the growth direction, and what may also be a chemical discontinuity. Strain discontinuity but no compositional gradient was reported in 120 nm thick $In_{0.19}Ga_{0.81}N$.[29] Liliental-Weber *et al.*[30] studied $In_{0.28}Ga_{0.72}N$ and $In_{0.40}Ga_{0.60}N$ epilayers using transmission electron microscopy (TEM) and correlated the double points to a self-formed pseudomorphic InGaN interlayer between the main film and the substrate, which was termed a "sequestration layer" (SQL) and had lower indium concentration (0.17 in the first case and 0.23 in the second). Contrary to the SQL, the main epilayer was very rich in basal stacking faults (BSFs). It also exhibited a saw-tooth surface structure. When the indium content was increased to 0.45, the SQL was suppressed but the BSFs and surface roughness persisted. However, in another study, of $In_{0.08}Ga_{0.92}N$ with ~30 nm thickness,[31] sequestration was observed despite that the thickness was far below critical. One sublayer had a 10 nm thickness and $x = 0.04$, whereas the second one had a 25 nm thickness and $x = 0.10$. In later work on low (0.10) indium content films, Liliental-Weber *et al.*[28] observed that the phenomena of surface roughening and BSF introduction became more intense with increasing film thickness, giving rise to polytype-like areas. Cho *et al.*[32] also observed saw-tooth surface roughening and introduction of multiple BSFs in epilayers with indium content between 0.18 and 0.45. However, although they reported that the InGaN region closer to the GaN substrate retains more elastic strain, they found a gradual and not discontinuous strain relaxation with increasing thickness, with most relaxation occurring between 20 and 50 nm thickness. In the study of Wang *et al.*,[33] sequestration was correlated to dislocation glide on pyramidal planes from the film surface. Pantzas *et al.*[34] employed Z-contrast imaging to view a 140 nm sequestrated $In_{0.2}Ga_{0.8}N$ film and found that the SQL contained $x = 0.13$ indium. Based on their Z-contrast quantification, they observed a stark compositional difference between the SQL and film, explained by the absence of compositional pulling. Wilsch *et al.*[35] found that indium remained constant at $x = 0.13$ up to ~100 nm and this layer was relaxed by 20%. Then, it increased up to $x = 0.19$ in the next 200 nm and saturated in the relaxed 100 nm thick upper part. Müller *et al.*[36] employed atom probe tomography in 300 nm $In_{0.25}G_{0.75}N$ to show that indium remains almost constant in the SQL (~40 nm thick) and then starts to increase gradually.

It has been suggested that the strain discontinuity of the SQL should be attributed to a transition from 2D growth to Stranski-Krastanow type 2D/3D growth and that it is invariably associated with the saw-tooth roughening of the film surface, which aids the incorporation of indium.[37–40] The sequestration phenomenon has also been observed in PAMBE-grown epilayers, but the relevant reports in films grown by this method are very sparse.[21,41]

Based on the afore-given literature review, there is no consensus on what actually takes place during the relaxation of InGaN films, i.e., if there is a strain or compositional discontinuity (or both) close to the InGaN/GaN interface or whether chemical and strain gradients are in place. Also, we do not understand clearly the onset of defect introduction and how critical thickness calculations need to be modified in order to take into account the dominant and distinct strain relaxation mechanism(s) that appear under the employed growth conditions, especially those of PAMBE growth. Elastic strain and indium surface kinetics constitute the primary driving forces for the realization of such phenomena. In this regard, it is important to achieve a deconvolution of the influences of growth conditions on these two factors and to elucidate the chemical and strain gradients taking place.

In our contribution, we focus on TEM observations of PAMBE-grown films deposited at different temperatures under constant fluxes. Hence, we monitor the changes that occur by influencing just one parameter that affects the indium mobility. We report on the correlation between the indium content (on average as well as along the growth direction) and the dominant strain relaxation mechanisms of the films. We demonstrate the change of relaxation mode with temperature and the gradual suppression of the SQL. We also analyze the line and extended defects that are introduced, and we elucidate the structure of the sequestration interface. Finally, we report on the correlation between strain relaxation and chemistry, and show that the chemical variation is gradual in the film but the strain variation is discontinuous. Based on our results, we propose that accomplishing early strain relaxation through indium saturation of the growth front is a prerequisite for suppressing the SQL.

II. EXPERIMENT

InGaN (0001) films were grown heteroepitaxially by radio-frequency PAMBE on commercial 2–4 μm thick MOVPE (0001) GaN-on-sapphire templates. The active nitrogen source was an Oxford HD-25 RF source employed in a Riber 32P MBE system. Group-III atoms were supplied from conventional Knudsen cells. InGaN growth was preceded by deposition of a 100 nm GaN buffer layer at standard conditions. The growth mode was monitored using reflection high energy electron diffraction (RHEED). We examined samples grown at different temperatures while keeping the III/N and In/Ga flux ratios constant. The total arrival rate of group-III atoms was above that of active nitrogen (N*) species, i.e., the growth conditions were slightly metal-rich. The corresponding arrival rates for Ga, In, and N* were 115, 135, and 235 GaN-equivalent nm/h, respectively. However, despite nominal conditions, surface stoichiometry is governed by the substrate temperature for constant flux ratios, due to indium desorption at higher temperatures. The growth temperatures ranged between $T_{gr} = 475$ and 590 °C. All samples were grown with the same deposition time.

TEM thin foil preparation for cross sectional observations along the $[11\bar{2}0]$ and $[1\bar{1}00]$ zone axes was performed by mechanical grinding using the tripod wedge polishing method in the Allied Multiprep, followed by ~15 min of Ar^+ ion milling in the Gatan PIPS. Cross sectional TEM (XTEM), plan view TEM (PV-TEM), and high resolution TEM (HRTEM) observations were performed using a 200 kV JEOL JEM 2011 microscope (point resolution 0.19 nm, $C_s = 0.4$ mm). High angle annular dark field (HAADF) observations for Z-contrast imaging were performed in a 200 kV FEI TECNAI G2 F20 S-TWIN scanning TEM (STEM). Energy dispersive x-ray spectroscopy (EDX) was performed using a 200 kV JEOL JEM 2010F microscope. Measurements of lattice constant variations at the nanoscale were obtained from HRTEM observations using geometrical phase analysis (GPA).[42] For GPA, negatives were digitized at 4000 dpi using a Nikon Super CoolScan 9000ED scanner. The sample surfaces were assessed by scanning electron microscopy using a JEOL JSM6390 LV microscope. High resolution XRD was performed using a Bede D1 diffractometer for the determination of the indium and strain content in the samples.

III. RESULTS

A. Average film properties, dislocation densities, and surface morphology

We have considered five samples grown at different temperatures that are listed in Table I. RHEED patterns remained streaky during growth in all samples, indicative of two-dimensional growth. There were no significant observable variations in the RHEED patterns during growth, except for sample E, for which the pattern gradually became less streaky, indicative of some surface roughening. Table I lists the average indium contents of the samples, as determined from lattice constant measurements using XRD and selected area electron diffraction (SAED). For the high resolution XRD measurements, the symmetric (0002) and asymmetric $(10\bar{1}5)$ Bragg reflections were employed for c and α lattice constant determination, respectively. SAED patterns were recorded along both the $[11\bar{2}0]$ and $[1\bar{1}00]$ zone axes, and results were averaged from at least three sample areas. For both methods, the indium concentration was then extracted by postulating that the epilayers abide to the condition of biaxial residual stress (the so-called "tetragonal distortion"). We also assumed that Vegard's law is valid, and performed this calculation in the manner described by Morales *et al.*,[43] using the GaN and InN lattice and elastic constants given therein. The lattice constants of InGaN were measured with reference to those of GaN. The InGaN elastic constants, as functions of the indium content, were obtained by linear interpolation from the respective constants of GaN and InN. Good agreement between SAED and XRD measurements was found, as can be seen in Table I. Furthermore, in all cases, the SAED patterns revealed a good heteroepitaxial relationship between epilayer and substrate, and no secondary phases.

TABLE I. List of samples grown by varying the growth temperature (T_{gr}), including average measurements of indium content (x_{In}), film thickness (h), total misfit (F), and strain relaxation (R).

	A	B	C	D	E
T_{gr} (°C)	590	580	565	535	475
x_{In} by XRD (±0.01)	0.12	0.18	0.27	0.36	0.42
x_{In} by SAED (±0.01)	0.11	0.17	0.26	0.38	0.41
h (±2 nm)	282	200	318	372	445
F (%)	−1.23	−1.87	−2.81	−3.98	−4.32
R (±5%)	39	70	73	90	86

A decrease of the indium content with increasing T_{gr} was recorded from the lattice constant measurements, which was attributed to indium desorption and InGaN decomposition. This trend was also reflected in the decrease, with increasing T_{gr}, of the film thickness, h, as determined by TEM and listed in Table I. Only sample A did not appear to abide to this trend, having a greater thickness than sample B, and the reason for this will be discussed in Section III B.

We have also listed in Table I the in-plane total misfit F, and the relaxation parameter R, defined as f/F, where f is the plastically relaxed strain. Since the films comprised different indium contents, R is a useful comparative measure of the percentage of plastic strain relaxation. Significant relaxation ($R \geq 70\%$) was observed at $x \geq 0.18$, whereas when indium exceeded 0.35, the films were almost fully relaxed ($R > 85\%$).

Regarding the structural quality of the films, Fig. 1 depicts XRD (0002) ω-2θ scans for all the samples. We observe that sample A exhibits clear phase separation with two distinct peaks. For samples B and C, we observe a grading of the (0002) lattice constant with formation of a shoulder-like region on the left hand side of the distributions. This could be attributed either to phase separation by compositional pulling or to strain relaxation following an initial

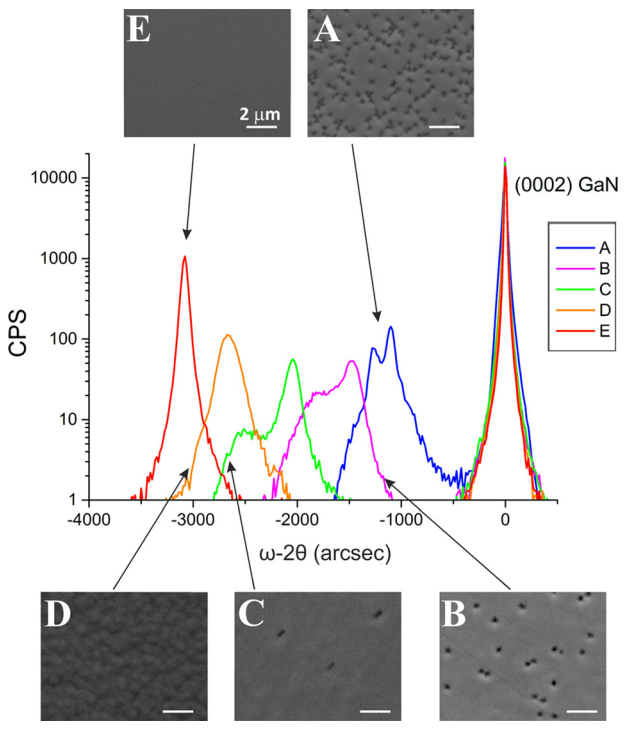

FIG. 1. High resolution XRD ω-2θ scans of the five samples around the (0002) Bragg point. Corresponding SEM micrographs are shown as insets.

high quality and low-indium content region that corresponds to the sharper peak on the right hand side of each angular distribution. This grading is reduced in sample D and disappears altogether in sample E. Elucidation of these findings requires structural observations using TEM and is undertaken in Section III B. Figure 1 also illustrates representative SEM images, given as insets, that depict the surface morphologies of the samples. It can be seen that the higher temperature sample A exhibited surface pits. These pits were significantly reduced in samples B and C and disappeared altogether in samples D and E. The pit density was reduced from $2 \times 10^8\,\mathrm{cm}^{-2}$ in sample A, to $2.5 \times 10^7\,\mathrm{cm}^{-2}$ in B and $3.8 \times 10^6\,\mathrm{cm}^{-2}$ in C.

Figure 2 gives the (0002) rocking curve FWHM obtained by XRD, in correlation with the density of TDs with **c**-type [0001] Burgers vector components as determined by TEM. The lowest values were obtained for samples A and E with $x = 0.11$ and 0.41, respectively, showing better crystal quality. It is noted that Burgers vector analysis by TEM using the **g.b** invisibility criterion showed that the TDs with **a**-type $1/3\langle 11\bar{2}0\rangle$ Burgers vector components were about three times more than those with **c**-type components.

Overall, the aforegiven comparative study of the films points to sample E as having the lowest defect density and better crystal quality. Detailed structural observations by TEM, given in Section III B, elucidate the strain relaxation processes taking place in correlation with the microstructure and the indium content of the films.

B. Defect microstructures

Following an order of decreasing T_{gr} in our presentation of the samples, the structure of the high temperature sample A is shown in the weak beam dark field (WBDF) XTEM images of Figs. 3(a) and 3(b). As can be seen in the image of Fig. 3(a), obtained with $g0002$, the pits on the sample surface (observed by SEM in Fig. 1) were V-pits associated with ascending TDs with **c**-type Burgers vector components that propagated from the GaN template. In fact, the V-pit density was almost the same as the TD density in the GaN substrate, i.e., almost all V-pits resulted from TDs coming from the substrate. The V-pits were deep, reaching close to the InGaN/GaN interface. Their surrounding film regions were decorated with **a**-type TD bundles, as can be seen in Fig. 3(b) obtained with g $1\bar{1}00$. On the contrary, the rest of the

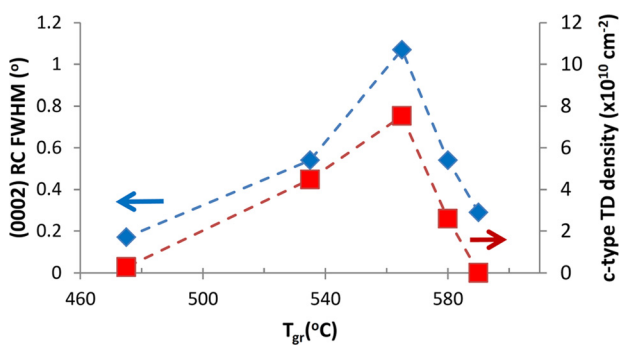

FIG. 2. Graphs of XRD (0002) rocking curve FWHM and **c**-component TD density versus the growth temperature T_{gr}.

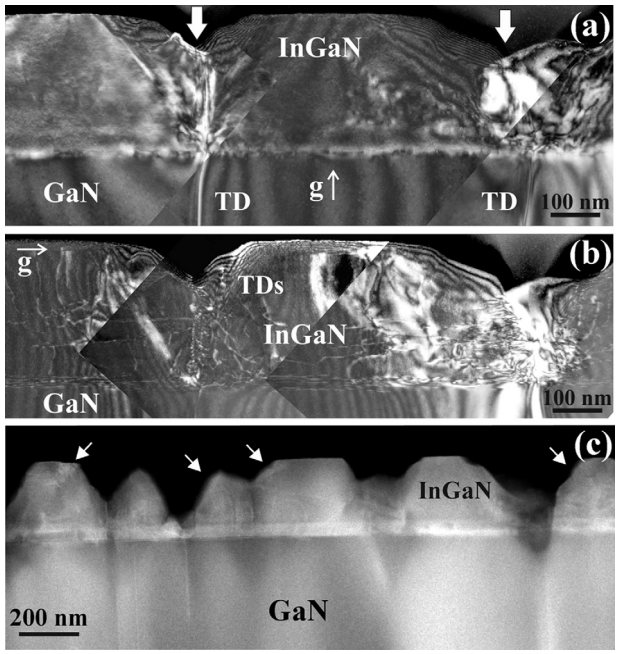

FIG. 3. (a) XTEM WBDF $g/3g$ image of sample A obtained near the $[11\bar{2}0]$ zone axis with $g0002$. Ascending TDs with **c**-type Burgers vector components coming from the GaN substrate open up to form V-pits. (b) Corresponding area obtained with g $1\bar{1}00$ under $g/3g$ conditions. (c) Z-contrast image showing an indium rich (bright) interfacial zone. Arrows indicate possible regions of high indium content at the facets of V-pits.

film exhibited low defect density. There were no regular misfit dislocation arrays, but we did observe **a**-type dislocations running parallel to the interface that contribute to the partial misfit relief. Such misfit dislocations may have nucleated at the V-pit areas.[23] There were several horizontal dislocations along the film height, which were connected to the TD bundles at the areas of the V-pits.

The localized defect formation at the V-pits of sample A can be attributed to the larger indium content there, compared to the rest of the film, leading to increased local strain. Indium adsorbs preferentially and is incorporated at the cores of the **c**-type TDs and at the $\{1\bar{1}01\}$ side facets of the V-pits.[44,45] Furthermore, the increased thickness of sample A, which was pointed out in Section III A, could be attributed to this preferential adsorption so that the growth rate for the rest of the film was closer to that of GaN. Another reason for the faster growth is the bunching of surface steps at the V-pits. The opening up of the V-pits started soon after the onset of InGaN growth, but further widening could also be attributed to the InGaN decomposition.

The indium distribution in sample A was examined using Z-contrast STEM imaging, as shown in Fig. 3(c). Regions of brighter contrast were observed at the facets of V-pits (as indicated by arrows), confirming the aforementioned indium segregation at these regions. However, what was striking is the appearance of a ~50–60 nm thick interfacial zone of abrupt brighter contrast, corresponding to higher indium content close to the heteroepitaxial interface. In order to determine the indium content inside this interfacial zone, we employed measurements of lattice constants from HRTEM images (not shown) using GPA. These measurements yielded an indium

concentration of $x = 0.14$, which is higher than the $x = 0.12$ found in the main film. This difference is consistent with the double XRD peaks shown in Fig. 1 and was further verified by EDX measurements on the same TEM foils.

Moving to sample B, we found that decreasing the growth temperature by 10 °C resulted in a drastic change of the strain relaxation mechanism, concurrent with the increase of the indium content by 0.06–0.07. As illustrated in Fig. 4, the prominent structural features of sample B were (a) the appearance of a SQL with low defect density and with average thickness of 40 nm and (b) the introduction of multiple BSFs immediately after this layer, similar to previous literature reports discussed in Sec. I. Contrary to the MOVPE layers, the film surface in our case was almost perfectly flat, and the sequestration phenomenon was not associated with a 3D growth mode. Figures 4(a) and 4(b) depict bright field (BF) XTEM images, obtained using $g0002$ and $g\ 1\bar{1}00$, respectively. It is seen that TDs were principally of **a**-type. Their density (as determined from PV-TEM observations) was equal to $1.3 \times 10^{11}\,\mathrm{cm}^{-2}$. Dislocations were also observed inside the GaN substrate, running parallel to the interface, as shown in Figs. 4(b) and 4(c). Such substrate dislocations have been reported previously in 200 nm thick $In_{0.12}Ga_{0.88}N$ grown by MOVPE[46] and could be related to strain partitioning between the film and the top substrate region. Regarding TDs with **c**-type Burgers vector components, new such defects were generated from the s-InGaN/GaN and InGaN/s-InGaN interfaces (whereby s-InGaN indicates the elastically strained InGaN in the SQL), as is visible in Fig. 4(a) and is attested by the dislocation density measurements in Fig. 2. However, the opening up of such TDs to V-pits was drastically reduced due to the lowering of T_{gr}.

Misfit dislocations were detected at the s-InGaN/GaN interface of sample B as illustrated in Fig. 4(c). This shows that the SQL was not fully elastically strained but partially relaxed. The misfit dislocations are projected inclined in Fig. 4(c) (arrowed) due to the two-beam imaging condition and thus become well visible. In order to elucidate their character, further observations were undertaken using PV-TEM, and Fig. 5 illustrates such an image from sample B. Three arrays of straight edge-type misfit dislocations aligned along the crystallographically equivalent $\langle 1\bar{1}00 \rangle$ directions were observed, revealing the operation of pyramidal slip systems during the formation of the SQL,[47] and thus confirming the postulate made by Wang *et al.*[33] On occasion, dissociations of these misfit dislocations were observed, as illustrated by black arrows in Fig. 5, showing that they may also bear 2**a** Burgers vector components.[47] The average spacing of the misfit dislocations in sample B was determined at $p = 292$ nm. Using the equation $f = -b/p$, where b is the magnitude of the Burgers vector, the plastic strain relaxation of the SQL was found equal to -0.11% corresponding to a lattice constant of $a = 0.3192$ nm for s-InGaN. In order to ascertain the indium content in the SQL of sample B, we also measured the c-lattice constant from cross sectional HRTEM observations using

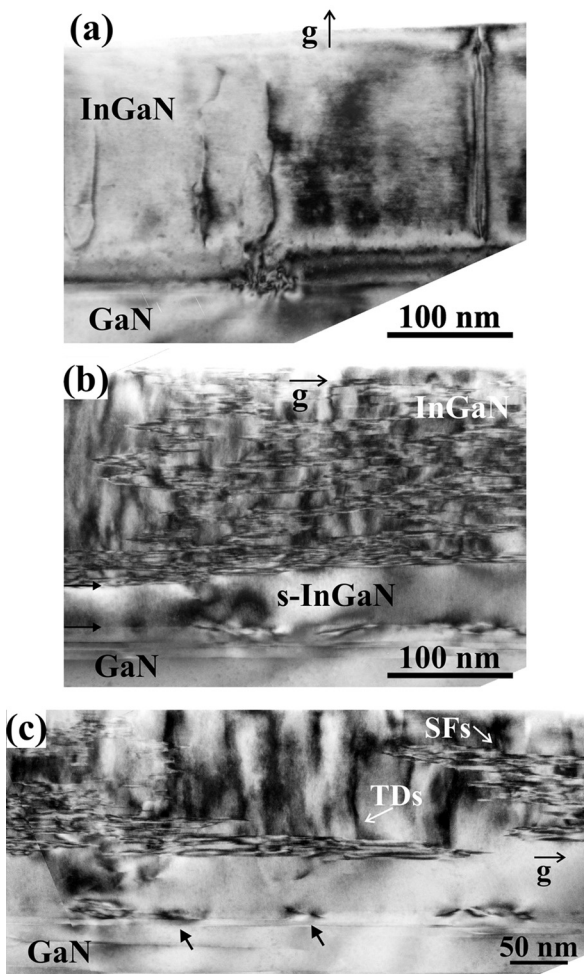

FIG. 4. (a) and (b) XTEM two-beam BF images of the same region of sample B, obtained near the $[11\bar{2}0]$ zone axis with $g0002$ and $g\ 1\bar{1}00$ conditions, showing TDs with **c**- and **a**-type Burgers vector components, respectively. Multiple BSFs are visible inside the InGaN film. The SQL, comprising elastically strained InGaN (s-InGaN), is clearly visible in (b). (c) Higher magnification from another film area showing the misfit dislocations at the s-InGaN/GaN interface (arrowed).

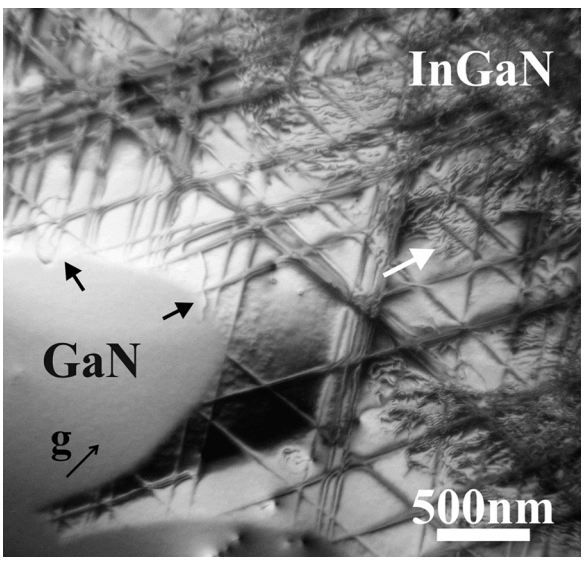

FIG. 5. Two-beam BF PV-TEM image of sample B, taken with $g\ 11\bar{2}0$, and showing misfit dislocations aligned along the $\langle 1\bar{1}00 \rangle$ directions. Black arrows point at dislocation dissociations. The white arrow shows curved dislocation segments towards the thicker part of the TEM foil, i.e., above the SQL. These are attributed to the TD half loops emanating from the SQL interface and BSFs (see text).

GPA, which gave a value of $c = 0.5317$ nm (i.e., 2.5% larger than GaN). Then, the biaxial stress approximation yielded a value of $x = 0.16$ for the average indium content in the SQL, i.e., slightly smaller than the average value of $x = 0.18$ for the whole film. It is worth pointing out that, for the given indium content of 0.16, the misfit dislocation spacing that is required for complete misfit relaxation is 21 nm, which is lower by one order of magnitude compared to the observed one. In the SQL of sample B, the elastic strain was -1.69%, and the relaxation parameter was $R = 6\%$. Compared to the average value of $R = 70\%$ for the whole film B, this shows that the SQL was almost fully elastically strained, and plastic strain relaxation principally commenced above it.

Samples C and D also exhibited a SQL. However, its thickness was found to be reduced to ~30 nm on average in sample C, as shown in Fig. 6(a). This took place through the gradual introduction of more BSFs closer to the InGaN/GaN interface. The SQL of sample D had a similar average thickness to that of sample C, despite its much higher indium content. However, the InGaN/s-InGaN interface was now more continuous and well-defined, as illustrated in Fig. 6(b). The SQL was fully eliminated in sample E, as shown in Fig. 6(c).

The SQL of sample D is illustrated in greater detail in the HRTEM image of Fig. 7(a). It can be seen that the InGaN/s-InGaN interface was a principal source of ascending TD half loops, revealing major plastic accommodation of elastic strain there. In all samples, the InGaN/s-InGaN interface was marked by an extended BSF that was discontinuous and stepped. Its character was determined by HRTEM/GPA and was found to be of I_1 type as shown in Fig. 7(b). The multiple BSFs that were introduced after this interface were also of I_1 type in their majority. Their distribution was inhomogeneous along the height and length of the film. More **a**-type TDs were found to be introduced from the steps and folds between these BSFs. Since the dominant BSF type is I_1, their emanation mechanism is not consistent with that proposed by Meng *et al.*,[48] which requires dissociation of Shockley partial dislocations and hence the existence of I_2 BSFs. The TD half loops emanating from the SQL interface and BSFs give rise to the curved dislocation segment contrast in plan-view observations, as indicated by the white arrow in the thicker parts of the TEM foil in Fig. 5.

As mentioned, in the low temperature sample E, the SQL was fully eliminated, and Fig. 7(c) is a characteristic HRTEM image of the InGaN/GaN interfacial region. Detailed structural observations revealed misfit dislocations at the InGaN/GaN interface, but no ordered dislocation array. In addition to the elimination of the SQL, BSFs were also eliminated almost completely in sample E, as can be seen in Figs. 6(c) and 7(c).

Regarding the transition from SQL to "no-SQL," our observations indicate that, with increasing indium content, the SQL gradually became decorated with **a**-type TDs. Such TDs were either introduced directly from the s-InGaN/GaN interface or from inside the SQL, as can be seen by comparing Figs. 4(b) and 6(a). Hence, it appears that the SQL/BSF mechanism was gradually overtaken by the introduction of more misfit dislocations at the s-InGaN/GaN interface, causing more plastic relaxation of the SQL. This leads us to consider that for a certain combination between strain and chemistry, there is a critical thickness for BSF introduction, relating to the accumulation of a critical amount of indium at the growth front. We address this issue in Section III C by combined GPA and EDX analysis.

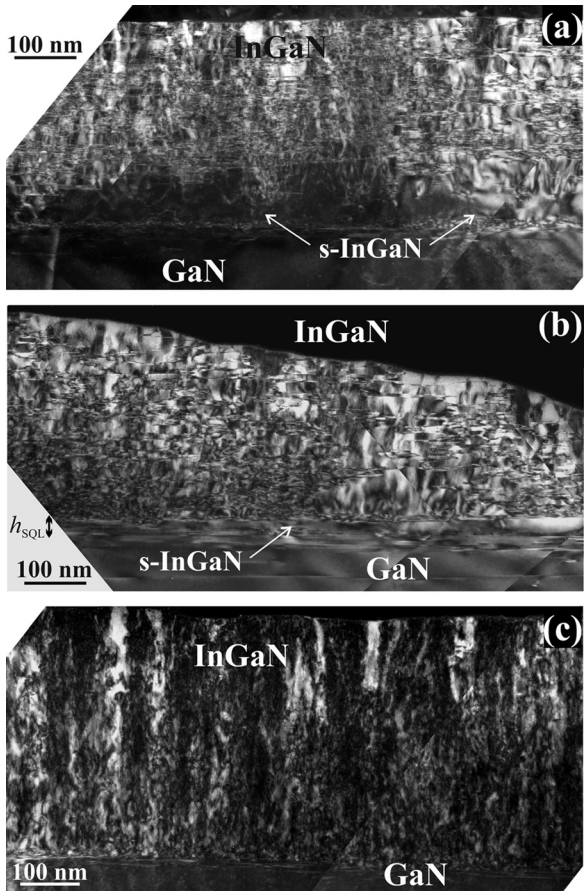

FIG. 6. (a) XTEM WBDF image of sample C obtained near the [11$\bar{2}$0] zone axis with g 1$\bar{1}$00 under $g/3g$ conditions. The SQL is seen to be "contaminated" with emanating TDs. (b) Similar XTEM WBDF image of sample D. The SQL interface is more continuous at a thickness of ~30 nm. (c) XTEM WBDF image of sample E obtained under similar conditions. No SQL is observable.

C. Compositional and strain profiling of sequestrated samples

As discussed in Sec. I, there has been a debate on whether the SQL is a rather chemically abrupt layer or if its composition varies gradually. Our Z-contrast imaging showed a darker contrast for the SQL compared to the rest of the film, similar to the observation of Pantzas *et al.*,[34] as illustrated in Figs. 8(a) and 8(b) for samples B and D, respectively. However, the brighter contrast above the SQL could signify not only a higher indium content but may also be attributed to the cores of the TDs that give rise to diffuse scattering, i.e., the high TD density could contribute to contrast formation even at high electron collection angles.[49,50] Similarly, the brighter s-InGaN/GaN interfacial contrast could be either due to the chemistry or associated with the misfit dislocations.

Therefore, we have employed EDX profiling in order to ascertain the average indium distribution along the growth

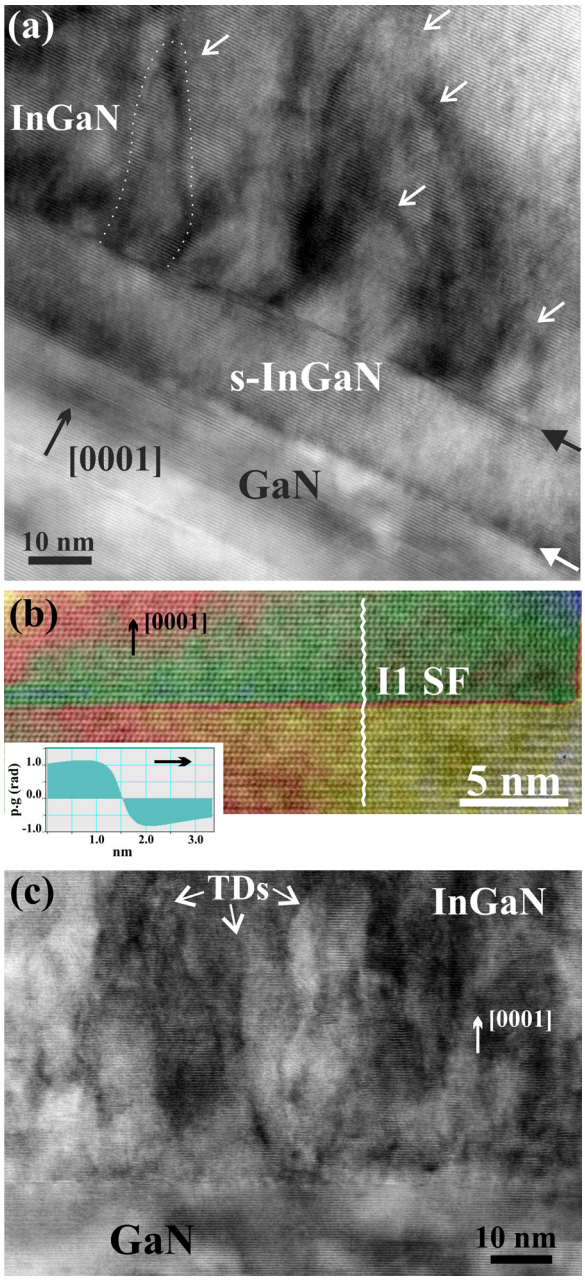

FIG. 7. (a) Cross sectional HRTEM image along [11$\bar{2}$0] showing emanation of TD half loops (white arrows) from the InGaN/s-InGaN interface (black arrow) in sample D. (b) HRTEM image with corresponding g 1$\bar{1}$00 phase map and phase profile across the InGaN/s-InGaN interface, obtained with ~0.5 nm spatial resolution. The phase change along the growth direction is given as inset. The [0001] growth direction is indicated in all images. (c) HRTEM image along [11$\bar{2}$0] of the interfacial region of sample E showing emanating TD half-loops from a rather distorted InGaN/GaN interface, and lack of BSFs in the InGaN film.

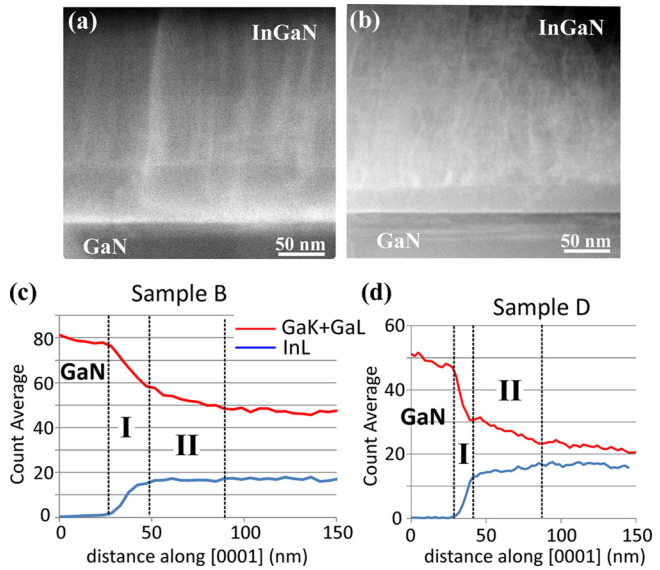

FIG. 8. (a) and (b) Z-contrast images of samples B and D, respectively. (c) and (d) EDX profiles along [0001] of the Ga and In lines, after noise subtraction, for samples B and D, respectively. Regions I and II in each case are delineated.

direction, without attempting a direct correlation with the Z-contrast images. Figures 8(c) and 8(d) illustrate EDX profiles along [0001] for samples B and D, respectively. The profiles have been obtained from 2D x-ray maps for the respective lines, after averaging for ~80 nm parallel to the interface. The maps were recorded with a ~2 nm spot size. What we can see for sample B ($x = 0.18$) is an initial interfacial region, roughly ~20 nm thick (region I) of rather abrupt change of the stoichiometry, followed by a more slowly graded region that extends for ~40 nm (region II). In other words, the chemical content is graded inside the SQL layer and stabilizes above it. A corresponding gradual strain increase was not detected here by HRTEM/GPA, probably because of the very small overall compositional change of 0.02.

Sample D ($x = 0.36$) also exhibited two compositionally graded regions. The interfacial one (region I) was ~10 nm wide, followed by a second region (region II), roughly ~40 nm wide, having a smaller compositional gradient before the film reached a steady-state indium concentration. It is noted here that some artificial broadening in the delineation of the interfacial region is unavoidable due to the influence of the excitation volume, despite the small probe size used. In any case, a real compositional sequestration in the form of chemical discontinuity does not seem to exist. Moreover, in sample D, the overall film thickness that exhibited compositional grading exceeded by almost two times the thickness of the visible SQL [Fig. 8(b)], contrary to the case of sample B where these thicknesses were rather close. This signifies that the critical thickness for the onset of BSF formation was reached before the end of the compositional pulling phenomenon in sample D.

Hence, BSF formation should be associated with a critical indium content and the resulting biaxial stress. In sample B, appearance of BSFs commenced when the indium content reached its final value close to 0.2. In order to ascertain if a similar indium content is associated with BSF introduction also in sample D, we undertook a detailed strain analysis of the first ~40 nm of epilayer thickness from HRTEM images using GPA. Figure 9 illustrates such a region with corresponding GPA for the g 1$\bar{1}$00 and g0002 spatial frequencies, depicting the reduced relative variations of the in-plane and out-of-plane InGaN lattice parameters with respect to that of GaN (expressed as "lattice strain", ε^{lt}). The GPA maps were collected using Gaussian masks placed around the respective spatial frequencies. The employed mask size was g/6, i.e., the spatial resolution was 1.6 nm for g0002 and 1.7 nm for g

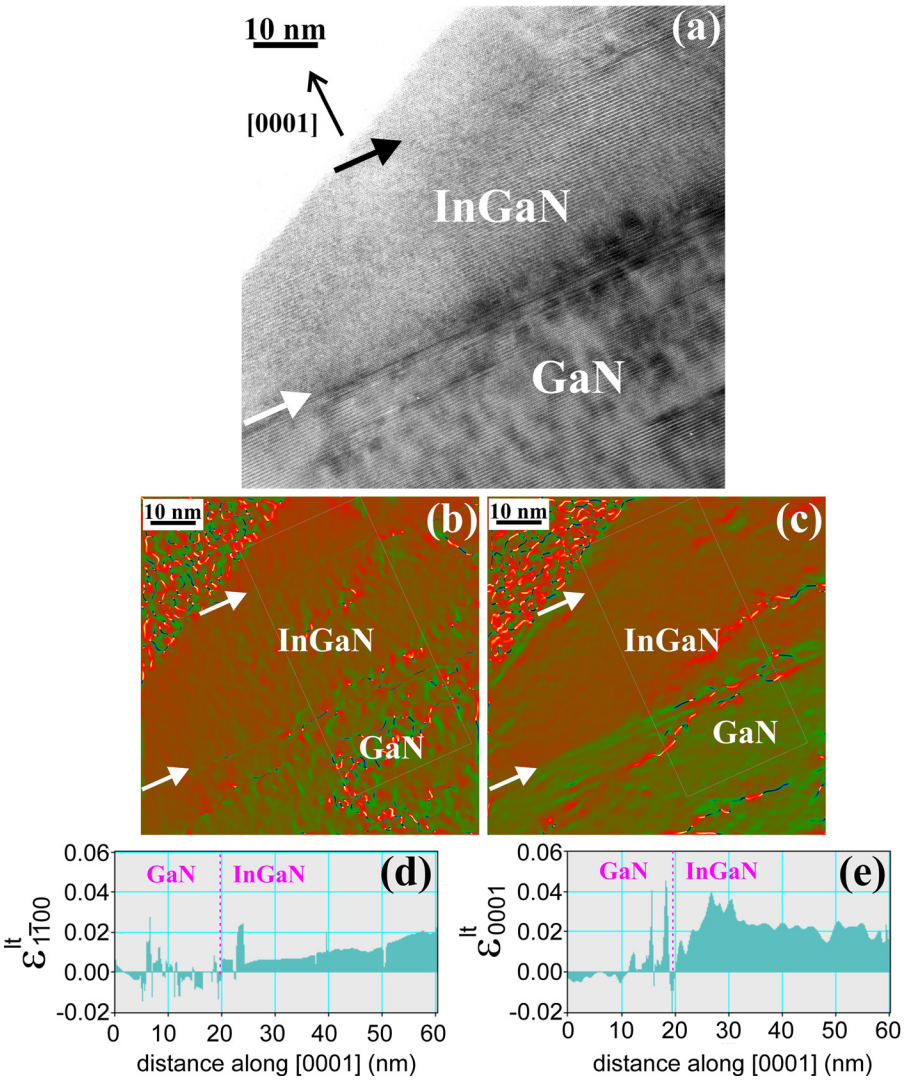

FIG. 9. (a) HRTEM image of the InGaN film close to the heteroepitaxial interface in the case of sample D. The white arrow indicates the s-InGaN/GaN interface, and the white arrow shows the InGaN/s-InGaN interface (BSF). (b) and (c) Corresponding GPA maps of the lattice strain along the $[1\bar{1}00]$ and [0001] directions, respectively. (d) and (e) Lattice strain profiles along the growth direction, obtained from (b) and (c), respectively.

$1\bar{1}00$. It can be seen that the *c*-lattice constant of the InGaN epilayer acquired almost abruptly the value of 2.2% greater than that of GaN. However, the *a*-lattice constant increased in a gradual manner, starting from 0.7% at the heteroepitaxial interface, and reached 2.0%, compared to that of GaN, just above the SQL. Assuming a biaxial stress state, this behavior is justified by a gradual increase of the indium content, starting from 0.16 at the interface and reaching 0.21 at the SQL discontinuity. This shows that BSF formation again commenced at a critical indium concentration of ~0.2, in agreement with sample B.

IV. DISCUSSION AND CONCLUSIONS

In the present work, we have focused on the observation of the strain relaxation mechanisms taking place during PAMBE growth while varying only the growth temperature under nominally slightly metal rich conditions. Prominent structural features were identified, and special emphasis was placed on the SQL, in correlation with the chemical distribution and defect introduction.

We found that, due to the strain relaxation through V-pit formation at higher T_{gr}, an indium rich interfacial zone was promoted in sample A. Although the observed indium configuration is reminiscent of that reported by Park *et al.*[51] for MOVPE-grown pyramidal InGaN (whereby the base region of the pyramids exhibited 0.89 indium content compared to 0.32 at the rest), in their case such regions were associated with the influence of ascending TDs. Here, we observed a laterally continuous indium-rich zone, and also its indium content was close to that of the epilayer. We postulate that the thickness of this interfacial zone actually reveals the h_{cr} for the opening up of the V-pits, since, up to that time, indium was incorporated homogeneously in the film. However, after formation of the V-pits, indium was incorporated preferentially there, hence the local introduction of TD bundles, as illustrated schematically in Fig. 10(a). Therefore, we may describe this growth as a modified Stranski-Krastanow mechanism, whereby an initial layer of higher indium concentration formed first. The interplay with the introduction of V-pits defined the second stage of the growth. We did not observe a strain-induced 3D growth mode since strain relaxation was accomplished through the opening up of TD cores, followed by preferential indium accumulation at these regions. The preferential indium segregation at the V-pits was probably the cause for the reduction of the indium content in the rest of the film.

This situation was reversed at lower growth temperatures, when the indium-deficient sequestration layer appeared, and

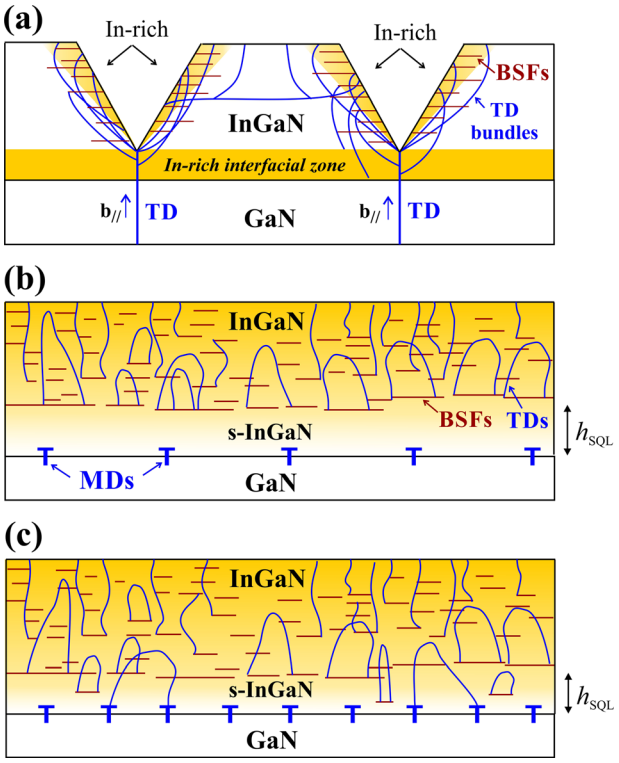

FIG. 10. Schematic illustration of the observed strain relaxation mechanisms shown in order of increasing indium content. (a) At lower indium contents, V-pit opening after formation of an indium-rich interfacial zone. (b) At intermediate indium contents, formation of a partially strained SQL (through misfit dislocations—MDs), and onset of major plastic strain relaxation through BSF formation above the SQL. (c) At higher indium contents, gradual suppression of the SQL through introduction of more misfit dislocations, and earlier formation of BSFs. TDs are introduced either from the misfit dislocations or from the BSFs (color grading indicates indium content).

V-pits gradually disappeared (samples B, C, and D). Contrary to previous reports on MOVPE-grown epilayers,[28,30,32,37–40] in our case (PAMBE), the sequestration phenomenon was not correlated to 3D growth. Hence, we do not support the argument that this phenomenon is a manifestation of a Stranski-Krastanow growth mode. This casts doubt on calculations showing that, up to the indium composition of 0.27, the critical thickness for 3D growth is smaller than that for dislocation generation through the Matthews-Blakeslee mechanism.[52] In our case, we observed partial relaxation even of the SQL through introduction of misfit dislocations, and our plan view observations (Fig. 5) indicate the operation of pyramidal slip planes.

Monitoring of the indium gradient along the growth direction of the films did not reveal a direct correlation between this gradient and the SQL thickness. After an initial steep rise, the indium content followed a gradual increase and saturated well below the final film thickness. The SQL was principally elastically strained, and the value of the in-plane strain inside the SQL was also graded. However, most of the elastic strain was plastically relieved at the SQL interface. In two representative studied samples, the SQL terminated when the indium content reached ~0.2. This critical indium content corresponded to an accumulated elastic strain energy that triggered the formation of multiple BSFs and associated partial dislocations that contributed to the strain relaxation process along the height of the film.[53] Thus, the SQL interface represented a discontinuity in the strain distribution along the growth direction, marking the boundary for the onset of plastic strain relaxation. However, our results did not confirm the claim of other authors that the SQL interface is a chemical interface between regions of low and high indium content.[34,36] Our observations regarding the SQL are summarized in Figs. 10(b) and 10(c). It is seen that at intermediate indium contents, the SQL is principally elastically strained since the critical indium content for BSF introduction is attained at an average thickness $h_{cr} = h_{SQL}$. Upon further increase of indium, h_{SQL} is reduced since the critical indium content is attained earlier. However, at the same time, more misfit dislocations are introduced early on. Hence, TD introduction also commences from the heteroepitaxial interface. At high indium contents, the plastic strain relaxation takes place almost fully at the InGaN/GaN interface and so there is no SQL and almost no BSFs.

The easy formation of I_1 BSFs is consistent with the low energy of this defect compared to the other stacking fault types.[54] However, their systematic formation cannot be explained on the basis of energetical considerations alone, but should be justified by the growth kinetics, i.e., the SQL probably has a kinetically defined critical thickness that is dependent on the combination of T_{gr} and elemental fluxes. In this respect, further experimental studies are required in order to clarify the influence of indium content (and hence strain) variation under constant T_{gr}, i.e., through variation of the fluxes. Based on the present results, we postulate that BSF formation is attributed to partial indium segregation to the growth front, leading to the formation of vacancy islands in the adlayer coverage.[55] Such islands accommodate extra indium atoms at their perimeter. The introduction of I_1 BSFs upon further growth probably also reduces the surface energy. Although explicit studies to this effect are not available to our knowledge, recent calculations by Duff *et al.*[56] show that indium surface atoms release strain energy by relaxing outwards, which may further promote BSF formation due to the small increase in the lattice parameter by the local transition from wurtzite to sphalerite structural units.[57]

By lowering T_{gr} under invariant fluxes, the thickness of the SQL was reduced as a result, in our opinion, of the earlier accumulation of the critical indium content. Concurrently, the SQL became more relaxed through the introduction of misfit dislocations at the heteroepitaxial interface. We postulate that, as the initial interfacial concentration of indium approaches the critical value, more misfit dislocations are generated there. Eventually, when this concentration is equal or greater than critical, the sequestration phenomenon is fully suppressed. Hence, the SQL suppression is correlated to the reduced indium desorption and early formation of an indium-rich surface adlayer. This is consistent with the observation of Liliental-Weber *et al.*[30] but, contrary to the MOVPE case, here BSF formation was also suppressed and 2D growth was maintained. The absence of BSFs in our sample E is intriguing, since, in fact, stacking errors should be favored at low T_{gr}. Therefore, it appears that not only the mobility of indium but also strain is relevant for the appearance of the BSFs. In the case of sample E, defect

introduction takes place early on at the heteroepitaxial interface, and then a steady state is maintained throughout the rest of the growth.

In summary, we have observed V-pit formation only at samples with lower indium contents and have associated this with a modified Stranski-Krastanow mechanism that can lead to slightly increased indium concentration in the first ~50 nm of film thickness. On the other hand, the sequestration phenomenon was observed under 2D growth, contrary to the MOVPE case. In PAMBE-grown films that exhibited sequestration, the chemical concentration along the film thickness saturated gradually, but was not in correspondence with the SQL thickness. The InGaN inside the SQL was partially elastically strained, depending on the amount of plastic relaxation that took place through misfit dislocations at the heteroepitaxial interface. This elastic strain increased from bottom to top of the SQL. The coupling between compositional pulling and strain relaxation resulted in the introduction of the SQL interface. This interface marks the onset of extensive plastic strain relaxation. The SQL thickness and indium content are kinetically defined depending on the pertinent growth conditions. Suppression of sequestration was achieved through early formation of an indium-rich adlayer.

ACKNOWLEDGMENTS

This research has been co-financed by the European Union (European Social Fund—ESF) and Greek national funds through the Operational Program "Education and Lifelong Learning" of the National Strategic Reference Framework (NSRF)—Research Funding Program: THALES, project NITPHOTO. J. S.-K. acknowledges support in the framework of Project BRIDGE: "Elimination of structural defects in nitride semiconductor layers (InGaN and InAlGaN) used as active layers in semiconductor lasers" funded by the Foundation for Polish Science in the frame of the EU operating program Innovative Economy.

[1]O. Jani, I. Ferguson, C. Honsberg, and S. Kurtz, Appl. Phys. Lett. **91**, 132117 (2007).
[2]C. J. Neufeld, N. G. Toledo, S. C. Cruz, M. Iza, S. P. Den Baars, and U. K. Mishra, Appl. Phys. Lett. **93**, 143502 (2008).
[3]I.-H. Ho and G. B. Stringfellow, Appl. Phys. Lett. **69**, 2701 (1996).
[4]D. Doppalapudi, S. N. Basu, K. F. Ludwig, and T. D. Moustakas, J. Appl. Phys. **84**, 1389 (1998).
[5]P. Ruterana and F. Deniel, Mater. Sci. Eng., B **59**, 186 (1999).
[6]F. A. Ponce, S. Srinivasan, A. Bell, L. Geng, R. Liu, M. Stevens, J. Cai, H. Omiya, H. Marui, and S. Tanaka, Phys. Status Solidi B **240**, 273 (2003).
[7]T. P. Bartel, P. Specht, J. C. Ho, and C. Kisielowski, Philos. Mag. **87**, 1983 (2007).
[8]N. El-Masry, E. L. Piner, S. X. Liu, and S. M. Bedair, Appl. Phys. Lett. **72**, 40 (1998).
[9]H. K. Cho, J. Y. Lee, C. S. Kim, G. M. Yang, N. Sharma, and C. Humphreys, J. Cryst. Growth **231**, 466 (2001).
[10]H. K. Cho, J. Y. Lee, and J. Y. Leem, Appl. Surf. Sci. **221**, 288 (2004).
[11]M. C. Johnson, Z. Liliental-Weber, D. N. Zakharov, D. E. McCready, R. J. Jorgenson, J. Wu, W. Shan, and E. D. Bourret-Courchesne, J. Electron. Mater. **34**, 605 (2005).
[12]D. I. Florescu, S. M. Ting, J. C. Ramer, D. S. Lee, V. N. Merai, A. Parkeh, D. Lu, E. A. Armour, and L. Chernyak, Appl. Phys. Lett. **83**, 33 (2003).
[13]H. Lei, J. Chen, and P. Ruterana, J. Appl. Phys. **108**, 103503 (2010).
[14]K. Hiramatsu, Y. Kawaguchi, M. Shimizu, N. Sawaki, T. Zheleva, R. F. Davis, H. Tsuda, W. Taki, N. Kuwano, and K. Oki, MRS Internet J. Nitride Semicond. Res. **2**, e6 (1997).
[15]Ž. Gačević, V. J. Gómez, N. G. Lepetit, P. E. D. Soto Rodríguez, A. Bengoechea, S. Fernández-Garrido, R. Nötzel, and E. Calleja, J. Cryst. Growth **364**, 123 (2013).
[16]M. Siekacz, M. Sawicka, H. Turski, G. Cywiński, A. Khachapuridze, P. Perlin, T. Suski, M. Boćkowski, J. Smalc-Koziorowska, M. Kryśko, R. Kudrawiec, M. Syperek, J. Misiewicz, Z. Wasilewski, S. Porowski, and C. Skierbiszewski, J. Apl. Phys. **110**, 063110 (2011).
[17]E. Monroy, B. Daudin, E. Bellet-Amalric, N. Gogneau, D. Jalabert, F. Enjalbert, J. Brault, J. Barjon, and L. S. Dang, J. Appl. Phys. **93**, 1550 (2003).
[18]E. Iliopoulos, A. Georgakilas, E. Dimakis, A. Adikimenakis, K. Tsagaraki, M. Androulidaki, and N. T. Pelekanos, Phys. Status Solidi A **203**, 102 (2006).
[19]K. G. Belyaev, M. V. Rakhlin, V. N. Jmerik, A. M. Mizerov, Y. V. Kuznetsova, M. V. Zamoryanskaya, S. V. Ivanov, and A. A. Toropov, Phys. Status Solidi C **10**, 527 (2013).
[20]T. Böttcher, S. Einfeldt, V. Kirchner, S. Figge, H. Heinke, D. Hommel, H. Selke, and P. L. Ryder, Appl. Phys. Lett. **73**, 3232 (1998).
[21]S. Valdueza-Felip, E. Bellet-Amalric, A. Núñez-Cascajero, Y. Wang, M.-P. Chauvat, P. Ruterana, S. Pouget, K. Loren, E. Alves, and E. Monroy, J. Appl. Phys. **116**, 233504 (2014).
[22]J. W. Matthews and A. E. Blakeslee, J. Cryst. Growth **27**, 118 (1974).
[23]B. Jahnen, M. Albrecht, W. Dorsch, S. Christiansen, H. P. Strunk, D. Hanser, and R. F. Davis, MRS Internet J. Nitride Semicond. Res. **3**, e39 (1998).
[24]S. Srinivasan, L. Geng, R. Liu, F. A. Ponce, Y. Narukawa, and S. Tanaka, Appl. Phys. Lett. **83**, 5187 (2003).
[25]R. Liu, J. Mei, S. Srinivasan, F. A. Ponce, H. Omiya, Y. Narukawa, and T. Mukai, Appl. Phys. Lett. **89**, 201911 (2006).
[26]R. People and J. C. Bean, Appl. Phys. Lett. **47**, 322 (1985).
[27]S. Pereira, M. R. Correia, E. Pereira, K. P. O'Donnell, C. Trager-Cowan, F. Sweeney, and E. Alves, Phys. Rev. B **64**, 205311 (2001).
[28]Z. Liliental-Weber, K. M. Yu, M. Hawkridge, S. Bedair, A. E. Berman, A. Emara, J. Domagala, D. R. Khanal, J. Wu, and J. Bak-Misiuk, Phys. Status Solidi C **6**, 2626 (2009).
[29]S. Pereira, M. R. Correia, E. Pereira, C. Trager-Cowan, F. Sweeney, K. P. O'Donnell, E. Alves, N. Franco, and A. D. Sequeira, Appl. Phys. Lett. **81**, 1207 (2002).
[30]Z. Liliental-Weber, M. Benamara, J. Washburn, J. Z. Domagala, J. Bak-Misiuk, E. L. Piner, J. C. Roberts, and S. M. Bedair, J. Electron. Mater. **30**, 439 (2001).
[31]K. S. Ramaiah, D. Huang, M. A. Reshchikov, F. Yun, H. Morkoc, J. Jasinski, Z. Liliental-Weber, C. Sone, S. S. Park, and K. Y. Lee, J. Mater. Sci.: Materials in Electronics **14**, 233 (2003).
[32]H. K. Cho, J. Y. Lee, K. S. Kim, and G. M. Yang, J. Cryst. Growth **220**, 197 (2000).
[33]H. Wang, D. S. Jiang, U. Jahn, J. J. Zhu, D. G. Zhao, Z. S. Liu, Z. S. Liu, S. M. Zhang, Y. X. Qiu, and H. Yang, Physica B: Condens. Matter **405**, 4668 (2010).
[34]K. Pantzas, G. Patriarche, D. Troadec, S. Gautier, T. Moudakir, S. Suresh, L. Largeau, O. Mauguin, P. L. Voss, and A. Ougazzaden, Nanotechnology **23**, 455707 (2012).
[35]B. Wilsch, U. Jahn, B. Jenichen, J. Lähnemann, H. T. Grahn, H. Wang, and H. Yang, Appl. Phys. Lett. **102**, 052109 (2013).
[36]M. Müller, G. D. W. Smith, B. Gault, and C. R. M. Grovenor, Acta Mater. **60**, 4277 (2012).
[37]S. M. de Sousa Pereira, K. P. O'Donnell, and E. J. da Costa Alves, Adv. Funct. Mater. **17**, 37 (2007).
[38]M. Leyer, J. Stellmach, C. Meissner, M. Pristovsek, and M. Kneissl, J. Cryst. Growth **310**, 4913 (2008).
[39]H. K. Cho, J. Y. Lee, and G. M. Yang, Appl. Phys. Lett. **80**, 1370 (2002).
[40]K. Pantzas, G. Patriarche, G. Orsal, S. Gautier, T. Moudakir, M. Abid, V. Gorge, Z. Djebbour, P. L. Voss, and A. Ougazzaden, Phys. Status Solidi A **209**, 25 (2012).
[41]V. N. Jmerik, A. M. Mizerov, T. V. Shubina, D. S. Plotnikov, M. V. Zamoryanskaya, M. A. Yagovkina, Ya. V. Domracheva, A. A. Sitnikova, and S. V. Ivanov, Semiconductors **42**, 616 (2008).
[42]M. J. Hÿtch, E. Snoeck, and R. Kilaas, Ultramicroscopy **74**, 131 (1998).
[43]F. M. Morales, D. González, J. G. Lozano, R. García, S. Hauguth-Frank, V. Lebedev, V. Cimalla, and O. Ambacher, Acta Mater. **57**, 5681 (2009).
[44]J. E. Northrup, L. T. Romano, and J. Neugebauer, Appl. Phys. Lett. **74**, 2319 (1999).

[45]Th. Kehagias, G. P. Dimitrakopulos, J. Kioseoglou, H. Kirmse, C. Giesen, M. Heuken, A. Georgakilas, W. Neumann, Th. Karakostas, and Ph. Komninou, Appl. Phys. Lett. **95**, 071905 (2009).
[46]Y. Zhang, M. J. Kappers, D. Zhu, F. Oehler, F. Gao, and C. J. Humphreys, Sol. Energy Mater. Sol. Cells **117**, 279 (2013).
[47]R. Liu, J. Mei, S. Srinivasan, H. Omiya, F. A. Ponce, D., Cherns, Y. Narukawa, and T. Mukai, Jpn. J. Appl. Phys., Part 2 **45**, L549 (2006).
[48]F. Y. Meng, H. McFelea, R. Datta, U. Chowdhury, C. Werkhoven, C. Arena, and S. Mahajan, J. Appl. Phys. **110**, 073503 (2011).
[49]J. M. Cowley and Y. Huang, Ultramicroscopy **40**, 171 (1992).
[50]T. Walther and C. J. Humphreys, "Quantification of the composition of silicon germanium/silicon structures by high-angle annular dark field imaging," in *Proceedings EMAG97 Cambridge*, edited by J. M. Rodenburg (Institute Physics Conference Series, Bristol, 1997), Vol. 153, pp. 303–306.
[51]J. Park, S.-I. Baik, D.-S. Ko, S.-H. Park, E. Yoon, and Y.-W. Kim, J. Electron. Mater. **38**, 518 (2009).
[52]W. Zhao, L. Wang, J. Wang, Z. Hao, and Y. Luo, J. Cryst. Growth **327**, 202 (2011).
[53]H. K. Cho and G. M. Yang, J. Cryst. Growth **243**, 124 (2002).
[54]C. Stampfl and C. Van de Walle, Phys. Rev. B **57**, R15052 (1998).
[55]H. Chen, R. Feenstra, J. Northrup, T. Zywietz, and J. Neugebauer, Phys. Rev. Lett. **85**, 1902 (2000).
[56]A. I. Duff, L. Lymperakis, and J. Neugebauer, Phys. Rev. B **89**, 085307 (2014).
[57]H. Morkoç, *Nitride Semiconductors and Devices: Fundamentals and Applications* (Wiley-VCH, 2013).